ELSEVIER

Experimental Study of the Performance Characteristics of a Steam-Ejector Refrigeration System

Yau-Ming Chen
Chung-Yung Sun
Department of Mechanical Engineering, National Taiwan University, Taipei, 10764, Taiwan

■ Conventional compression-refrigeration systems not only consume a large amount of electric power, but also cause serious environmental pollution. Among the various possible approaches in overcoming these two problems, a steam-ejector refrigeration system is believed to be most effective. This paper experimentally investigates the controlling parameters of a steam ejector, including operating conditions and the exit Mach number of the primary nozzle. Operation maps useful to the practical design are constructed from experimental results, and the empirical equations are correspondingly derived. Excessively increasing the exit Mach number of primary nozzle is unnecessary, and 4.35 should be a moderate value. With regard to the performance characteristics of the ejector itself, a steam ejector is better than an R114 ejector and is comparable to an R113 ejector. Moreover, with the use of a two-stage ejector, the required pressure to drive a steam ejector is reduced, and the low-grade heat source can be efficiently used. The results of primitive observation of the flow field are also discussed in this work. © Elsevier Science Inc., 1997

Keywords: *steam ejector, refrigeration, two-stage ejector*

INTRODUCTION

Currently, compression-refrigeration cycles are used mostly in air conditioners owing to their compactness and efficiency. However, the compressor is a large power-consuming compartment. In residential or office buildings, the compressor often places a heavy load on the electricity supply, especially in the summer. Therefore, greater emphasis must be placed on the research and development of nonmechanical refrigeration systems in which geothermal, solar, or waste heat can be used as the driving heat source.

Generally, the absorption machine is classified as the first type of nonmechanical refrigeration system. However, the initial investment in such a cycle is too high, and its maintenance is a rather specialized task, so its economic feasibility is limited. The ejector refrigeration cycle is classified as the second type. Zeren et al. [1] considered the commercial potential of the solar-driven ejector cycle with R12 as the refrigerant. They concluded that the efficiency of such a system depended mainly on the availability of a free solar heat source. Chen and Hsu [2] conducted a theoretical analysis of an ejector-compression heat pump cycle with R11 as the refrigerant. The estimated coefficients of performance are about 0.3 at practical operating conditions for air conditioning. Sokolov and Hershgal [3–6] undertook a series of work that experimentally and theoretically investigated the operation performance of Freon (R114)-ejector refrigeration systems. They used a booster and a two-stage ejector with an intercooler to enhance the system efficiency. In the research of Chen [7], the solar-driven ejector refrigeration system with R113 or R114 as the refrigerant was considered. In addition to the experimental study, they used the MacCormack TVD scheme to numerically calculate the flow field of ejector. However, there were still some discrepancies between the results of experiment and numerical analysis.

In addition to the problem of electricity supply, the use of refrigerants—mainly Freon—is another considerable problem in the operation of refrigeration systems. Chloroflurocarbon (CFC) refrigerants, such as R11, R12, R113, and R114, have been found to be seriously harmful to the ozone layer, and their uses are now restricted. Accordingly, the ejector refrigeration system with steam as refrigerant would be an attractive alternative for overcoming the two aforementioned problems.

The steam-ejector refrigeration system has many outstanding advantages, including simplicity, freedom from vibration, high reliability, and low operation and maintenance costs [8]. Therefore, it is used in a variety of

Address Correspondence to Prof. Yau-Ming Chen, Department of Mechanical Engineering, National Taiwan University, Taipei, Taiwan 10764.

Experimental Thermal and Fluid Science 1997; 15:384–394

655 Avenue of the Americas, New York, NY 10010

0894-1777/97/$17.00
PII S0894-1777(97)00006-X

applications, such as the freeze-drying process of preserving food, the crystallization of chemicals, and air conditioning. As illustrated in Fig. 1, an ejector refrigeration cycle basically consists of two subcycles: one is the power subcycle (1)-(2)-(3)-(4)-(5)-(1) and the other is the refrigeration subcycle (3)-(4)-(5)-(6)-(3). The pump is the only system compartment containing moving parts. It differs from the conventional Rankine refrigeration cycle in which the mechanical compressor is replaced by an ejector. The high-pressure vapor (2) provided by the generator is allowed to expand through a (typically converging-diverging) nozzle in the ejector. The low pressure produced by this expansion causes suction of vapor from the evaporator (3). The two streams mix in the ejector and then enter the diffuser part where the kinetic energy is converted back into an enthalpy increase. The resultant stream (4) leaving the ejector is condensed by a condenser.

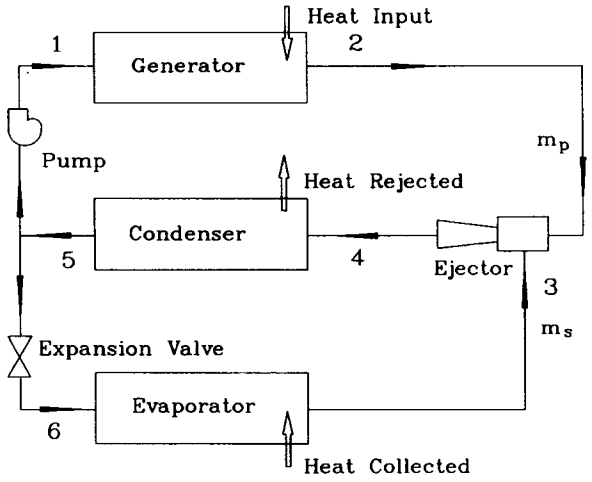

Figure 1. Schematic view of ejector refrigeration cycle.

The steam ejector was first used by LeBlanc and Parsons [8]. Many papers investigating the ejector characteristics have been published, most of which have concerned analysis of air-to-air [9–11], steam-to-air [12, 13], or other combinations [14, 15]. Through the efforts of these researchers, we have a better understanding of ejectors. However, the applicability to steam-to-steam ejectors seems to be questionable. Furthermore, the very complicated flow structure inherent in the supersonic steam ejector makes it difficult to precisely predict the ejector behavior by means of simplified theoretical analysis. Moreover, although ejector manufacturers possess much valuable experimental data, they are understandably reluctant to publish this data.

To experimentally investigate the performance characteristics of the steam-ejector refrigeration cycle, a relatively small scale system was built and tested at various operating conditions—namely, primary-flow pressures, secondary-flow pressures, and back pressures of the ejector. The effects, including the exit Mach number of the primary nozzle and the two-stage ejector, also are discussed. In addition, a transparent ejector was designed to primitively observe the flow field and, for future work, examine the flow structure by using the holographic interferometry method.

EXPERIMENTS

Apparatus

A schematic representation of the experimental setup is shown in Fig. 2. The apparatus consists mainly of a steam generator, a superheater, an ejector, an evaporator, a condenser, a water receiver, a liquid pump, and measuring devices. The steam generator is equipped with a 12-kW heating element and a safety valve. A SCR controller is used to control the temperature to within ± 0.1°C. A vapor-liquid separator was installed between the genera-

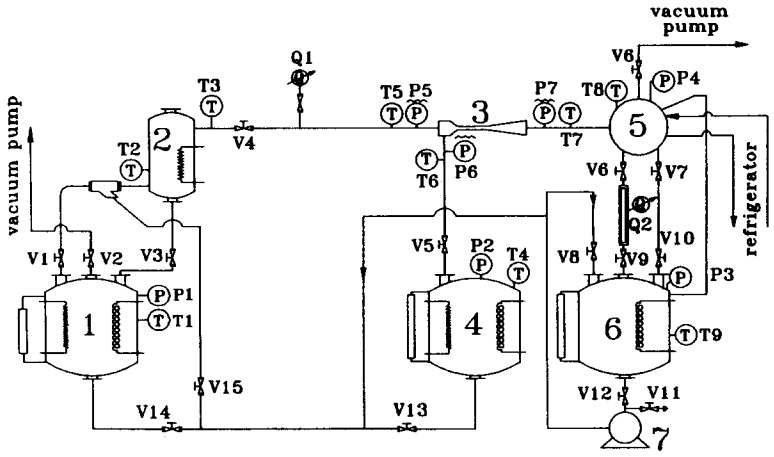

flowmeters (Q1–Q2)
thermocouples (T1–T9)
pressure gauges (P1–P4)
pressure transducers (P5–P7)
control valves (V1–V15)
vapor–liquid separator
heating element
cooling coil

Figure 2. Schematic description of experimental setup: (1) generator; (2) superheater; (3) ejector; (4) evaporator; (5) condenser; (6) water receiver; (7) liquid pump.

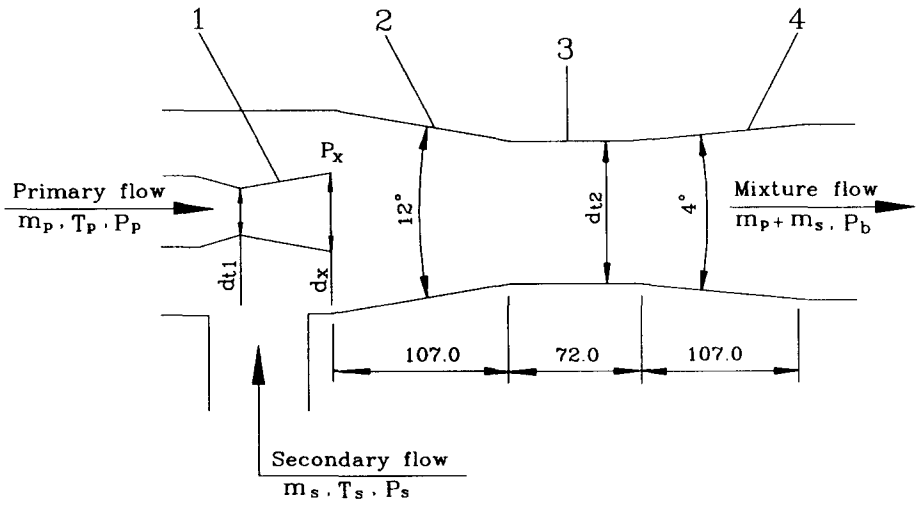

	Ejector 1	Ejector 2	Ejector 3
dt1	5.8	2.0	1.4
dt2	17.8	17.8	17.8
dx	12.5	9.3	8.7

unit : mm

Figure 3. Configuration and dimensions of ejector; (1) primary nozzle; (2) mixing section; (3) constant area section; (4) diffuser section.

tor and superheater. The high pressure vapor leaving the superheater is about 1–2°C of superheat. The evaporator is equipped with a 6-kW heater controlled by a SCR controller to within ±0.1°C. The exit mixture vapor from the ejector is condensed in a shell-and-tube condenser having a 2.0-m^2 heat transfer area. The cooling water used in the condenser is provided by a 5-ton refrigeration capacity chiller. A PID controller is used to control the condensing temperatures to within ±0.2°C, thus adjusting the back pressures of the ejector. Figure 3 shows the configuration of the ejector used, which is the most important compartment of the system. The corresponding geometric dimensions also are listed in Fig. 3. According to the work of Huang [16], the location of the primary nozzle significantly affects system performances, and the optimum position of the primary nozzle exit is at the entrance plane of the mixing section. In the present work, three sizes were designed for testing [13]. If isentropic and one-dimensional flow is assumed, the exit Mach numbers of the primary nozzle are 2.70, 4.35, and 5.0 for ejectors 1, 2, and 3, respectively. In addition, the wall pressures of the ejector were measured by six pressure sensors 80, 115, 170, 195, 230, and 265 mm from the inlet of the mixing section.

The sheath thermocouples were installed in the desired locations (T1–T9) for temperature measurement. Calibration of the thermocouples indicates the accuracy to within ±0.1°C. Variable capacitance-type pressure transducers (P6, P7) were installed in the inlet of the secondary flow and the exit of the ejector to measure their absolute vacuum pressures. The accuracy of such a sensor is ±0.25% of the full scale (100 torr). The inlet pressure of the ejector was measured by a strain-gauge pressure transducer (P5) whose accuracy is ±0.1% of the full scale (10 kgf/cm^2). Solid-state pressure sensors were used to measure the wall pressures with an accuracy of about ±1.0 torr. The primary flow rate was measured by a differential pressure-type flow meter that uses the theory of the conservation of energy in a fluid flowing through a pipe of specific design. After calibration the accuracy of this flow meter is ±1.0% of the reading value. Considering the low absolute pressure of the secondary vapor flow, we did not try to measure its flow rate directly. Instead, a marked glass tube of 25.4-mm i.d. and 300-mm length was installed under the condenser to collect the mixture water flow leaving the condenser. The time period for the liquid level to reach the bottom and top marks of the glass tube was measured by a digital timer. Then the mixture flow rate can be simply calculated by dividing the time period into the known volume between the two marks. Accordingly, the secondary mass flow rate was obtained by subtracting the primary mass flow rate from the mixture mass flow rate.

Experimental Procedure

The experimental system is first evacuated by a vacuum pump until its pressure is equal to the saturation pressure corresponding to the water temperatures at the generator and evaporator. The tap water in the generator is then heated to generate the driving high-pressure vapor. Before the SCR-controlled heater of the evaporator is turned on, the tap water in the evaporator is initially cooled to the required temperature by a 2-ton refrigeration capacity chiller. The high-pressure vapor (primary flow) enters the primary nozzle of the ejector and induces the low-pressure vapor (secondary flow) from the evaporator. The mixture vapor formed is condensed in the condenser and flows down into the water receiver by gravity. When the steady-state condition is reached (after about 10 min), the corre-

sponding flow rate, temperatures, and pressures are recorded. At this point, valves V7 and V9 are closed and valve V6 is opened to measure the mixture flow rate several times, as described in the preceding section.

The batch-type experimental system is designed to run at least 1 h. After one experiment has been conducted, valves V12–V14 are opened and the others are closed. The water in the receiver is then pumped back to the generator and evaporator to restart another experiment.

Experimental Uncertainty

Uncertainties in three diameters of the ejector, d_{t1}, d_{t2}, and d_x, are less than $\pm 5.0\%$. A detailed error analysis based on the inaccuracies in the measurement of temperature, volume between two marks of the glass tube, and the time period shows the maximum uncertainty in the calculated value of the mixture mass flow rate to be $\pm 3.7\%$. From the error in the measurement of the mixture mass flow rate and the primary mass flow rate, the uncertainties in the secondary mass flow rate and the entrainment ratio are determined to be $\pm 5.0\%$ and $\pm 6.2\%$, respectively.

RESULTS AND DISCUSSION

The coefficient of performance (COP) of a refrigeration cycle is defined as the ratio between the generated refrigeration and the energy input into the cycle. Let Q_e and Q_g be the heat-exchange rates in the evaporator and generator. Let W_{mec} be mechanical power required by the cycle (by the pump). The COP of the ejector refrigeration cycle is then defined as

$$\begin{aligned} \text{COP} &= Q_e/(Q_g + W_{mec}) \\ &= m_s \times \Delta h_e/(m_p \times \Delta h_g + W_{mec}) \end{aligned} \quad (1)$$

Here, Δh_e and Δh_g are enthalpy differences in the evaporator and generator, and m_s and m_p are the mass flow rates of the secondary vapor and primary vapor, respectively. In the ejector refrigeration cycle, W_{mec} can be neglected compared with the energy required in the generator. The entrainment ratio ω of the ejector is defined as

$$\omega = m_s/m_p. \quad (2)$$

Accordingly, the COP of the cycle can be rearranged as

$$\text{COP} = \omega \times (\Delta h_e/\Delta h_g). \quad (3)$$

Therefore, the entrainment ratio is an important parameter in the evaluation of the performance characteristics of ejector refrigeration cycles.

The present study relates to the following parameters: (1) the primary-flow pressure, P_p; (2) the secondary-flow pressure, P_s; (3) the back pressure of the ejector, P_b; and (4) the exit Mach number of the primary nozzle, Ma. The range of parameters covered during experimentation are given in Table 1.

Effect of Back Pressure of Ejector

Figure 4*a* shows how the entrainment ratio ω varies with the back pressure of the ejector, P_b. The exit Mach number, Ma, is 4.35 and the primary-flow pressure, P_p, is 1.98 bar. The secondary-flow pressure, P_s, is 9.8 torr (the corresponding saturation temperature $T_s = 11.0°C$), which

Table 1. Range of Experimental Parameters

	P_p	P_s (torr)	P_b (torr)
Ejector 1 ($Ma = 2.70$)	89.3, 116.0, 146.8 186.3 torr	7.5, 9.8, 13.6	10.0–50.0
Ejector 2 ($Ma = 4.35$)	1.16, 1.53, 1.98, 2.70 bar	9.8, 14.5, 17.6	10.0–50.0
Ejector 3 ($Ma = 5.00$)	4.23, 4.89, 5.46, 6.10 bar	9.2, 12.5, 17.6	10.0–50.0

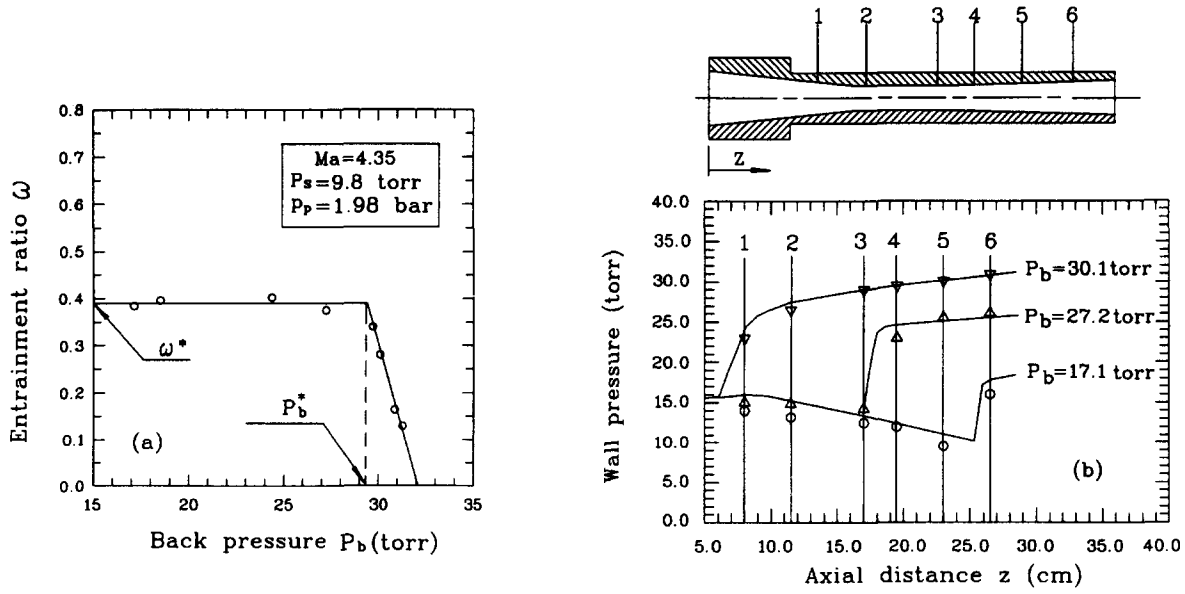

Figure 4. (*a*) Effect of back pressure of ejector. (*b*) Distribution of wall pressure along axial direction.

is almost the same as that of the evaporator. As shown in Fig. 4, the secondary vapor flow begins to be entrained by the ejector when the back pressure is brought down to about 32 torr. The entrainment ratio increases first, with a decrease of the back pressure in the range of about 29.3–32.0 torr, and then ω remains virtually constant. These two limited values are respectively termed the critical back pressure, P_b^*, and the critical entrainment ratio, ω^*, as shown in Fig. 4*a*.

Figure 4*b* presents the variations in the ejector wall pressure along the axial direction. At $P_b = 17.1$ torr, there is an obvious wall pressure jump between measurement points 5 and 6, and the corresponding entrainment ratio is said to be ω^*. It seems to be implied that the resultant flow proceeds at sonic speed in the constant area section, and an oblique shock appears in the diffuser section that causes a sudden pressure increase. As the back pressure increases to 27.2 torr (slightly smaller than P_b^*), the wall pressure jump moves upstream to between the measurement points 3 and 4. In addition, the pressures in front of the jumps do not change with the back pressures. These two limited cases represent the choking condition associated with the entrained flow rate of the secondary flow from the evaporator not being affected by the back pressure. When the back pressure further increases to 30.1 torr, exceeding P_b^*, the oblique shock is pushed to pass through the constant area section. As a result, the constant area section is not in the choking condition, and the entrainment ratio has begun to decrease below ω^*. Therefore, P_b^* would be the critical value at which an oblique shock occurs right at the entrance plane of the diffuser section. Below this value, the choking (sonic) condition is attained at the constant area section and the entrainment ratio would become independent on the back pressure. In other words, P_b^* is the maximum back pressure needed to obtain a critical (stable) entrainment ratio ω^*.

Effect of the Pressure of Primary Flow

Figure 5 plots the entrainment ratio against the back pressure of the ejector for four tested primary-flow pressures, P_p. The exit Mach number, *Ma*, is 4.35 and the secondary-flow pressure, P_s, remains constant at 9.8 torr. The variations of ω with P_b for these four values of P_p are similar, as described in the preceding section. Let P_x be the discharged pressure of the primary nozzle. For a given supersonic primary nozzle, the pressure ratio P_x/P_p will remain almost constant such that an increase in P_p will cause a subsequent increase of P_x, resulting in a decrease of the pressure difference $P_s - P_x$. Obviously, a lower $P_s - P_x$ would yield a less-entrained flow rate from the evaporator. Therefore, ω^* would decrease as the primary-flow pressure increases. On the other hand, a larger P_p would push the oblique shock wave occurring in the diffuser section more downstream, thus increasing the shock intensity. Consequently, the critical back pressure is increased by increasing P_p, which would be useful for the condenser operation in the refrigeration cycles.

Effect of Pressure of Secondary Flow

The pressure of secondary vapor flow, P_s, is another controlling parameter for the ejector performance. Figure 6 presents the entrainment ratio as a function of the back pressure at three values of P_s for a given $P_p = 1.98$ bar. The variations of ω with P_b for the three tested values of P_s are qualitatively similar to the curves depicted in Fig. 5; that is, a sharp decrease in the ejector entrained rate

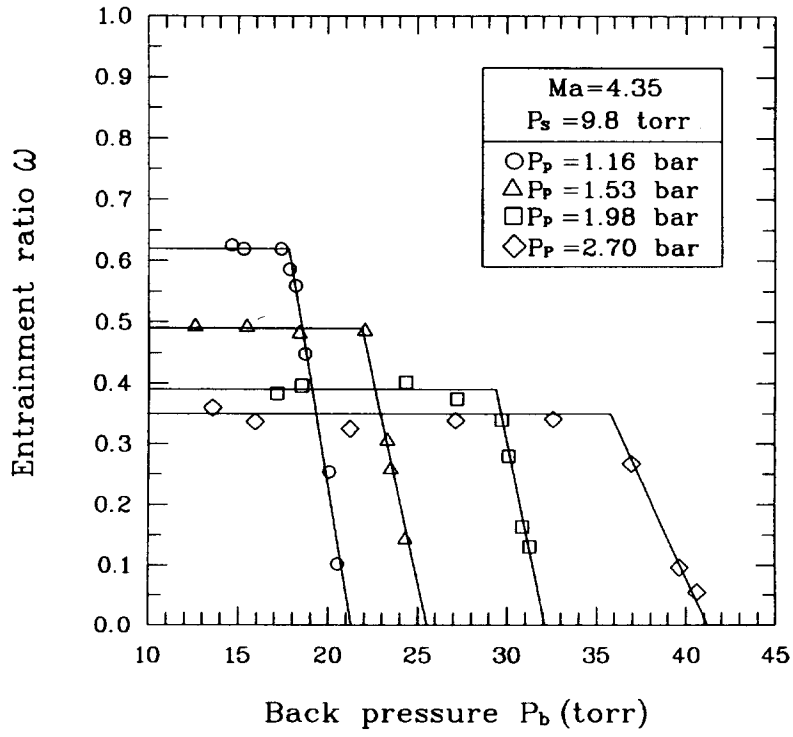

Figure 5. Effect of pressure of primary flow.

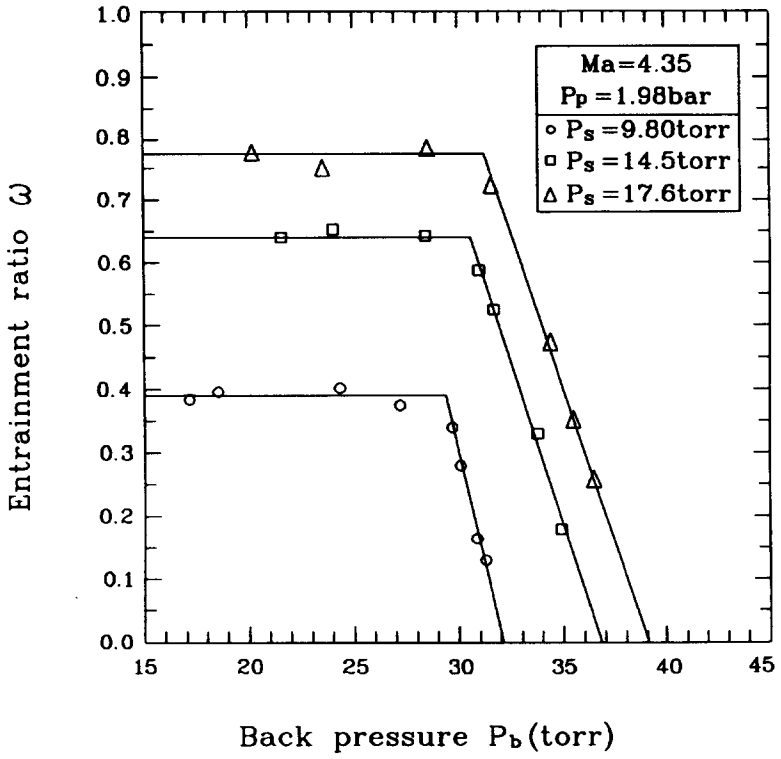

Figure 6. Effect of pressure of secondary flow.

when P_b exceeds the critical back pressure. An increase in P_s would always cause an increase in the driving pressure difference $P_s - P_x$ for the given P_p and Ma and thereby increases the entrainment ratio. Furthermore, increasing the secondary-flow pressure would increase the critical back pressure for a reason similar to that described in the preceding section. Although a larger secondary-flow pressure has the advantages of increasing both ω^* and P_b^*, the increase in P_s is limited by the saturation water temperature for the practical use of a refrigeration system.

Discussion and Comparison of Performance Characteristics of an Ejector

The back pressure of the ejector is nearly the same as that of the condenser, provided that the pipe length between the ejector and condenser is short enough. The condenser pressure and its corresponding saturation temperature are determined by the cooling-water temperature required for cooling purposes. In other words, the back pressure of the ejector is directly controlled by the cooling-water temperature. Usually, the cooling-water temperature should be less than the saturation temperature of vapor entering the condenser at the condenser pressure by at least 5°C. This is normally limited by the water available for cooling. On the basis of this consideration, the critical back pressure, P_b^*, determined previously is an important value for practical operation.

Figure 7 plots the variations of P_b^* with the corresponding critical entrainment ratio ω^* at different operation conditions—say, P_s and P_p. The solid lines (1–4 and a–d) represent the cases in which the ejector is running at a given value of P_p for different P_s, and the dashed lines (5–7 and e–g) represent those at a given value of P_s for different P_p. The constructed maps can be viewed as the operation maps for the ejectors tested here. As shown in Fig. 7, the extent of the effect of P_p on P_b^* is larger than that of P_s on P_b^*; however, the effects of P_p and P_s on ω^* are similar. A comparison of operation maps obtained for different Ma reveals that the critical entrainment ratios for $Ma = 4.35$ are always larger than that for $Ma = 2.70$ at a given critical back pressure. In other words, the ejector operating at a higher Ma has the better performance characteristics. However, to what extent should the exit Mach number be increased? As shown in Fig. 8, the effect of increasing Ma from 2.70 to 4.35 on the critical entrainment ratio is more pronounced than that of increasing Ma from 4.35 to 5.0. For a given critical compression ratio, such as $P_b^*/P_s = 3.2$, the critical entrainment ratios are 0.15, 0.35, and 0.40 for $Ma = 2.7$, 4.35, and 5.0, respectively. Although ω^* is slightly increased by increasing Ma from 4.35 and 5.0, the required P_p is greatly increased by about three times. The higher driving pressure means higher initial and running costs for ejector operation. Therefore, it seems to be unnecessary to excessively increase the exit Mach number, 4.35 should be a moderate value for practical operation of a steam ejector.

From a summary of experiment results, the following empirical equations are derived by the power regression method in the current experimental ranges:

1. $Ma = 5.0$

$$P_p/P_s = 125.5(P_b^*/P_s) - 26.80, \quad 150 < P_p/P_s < 500, \tag{4}$$

$$\omega^* = 4.806 - 3.858(P_b^*/P_s) + 1.150(P_b^*/P_s)^2 - 0.117(P_b^*/P_s)^3 \tag{5}$$

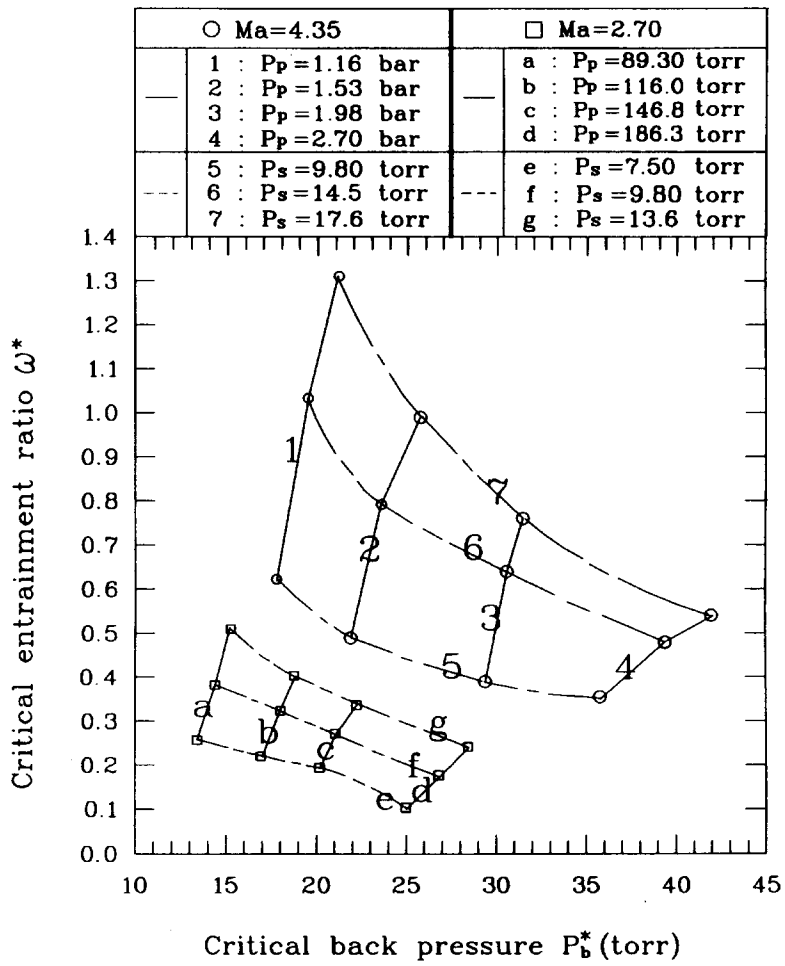

Figure 7. Variation of critical entrainment ratio with critical back pressure for different operating conditions.

2. $Ma = 4.35$

$$P_p/P_s = 60.13(P_b^*/P_s) - 23.09, \quad 50 < P_p/P_s < 250, \tag{6}$$

$$\omega^* = 3.018 - 2.206(P_b^*/P_s) + 0.640(P_b^*/P_s)^2 - 0.066(P_b^*/P_s)^3 \tag{7}$$

3. $Ma = 2.70$

$$P_p/F_s = 8.652(P_b^*/P_s) - 3.671, \quad 5 < P_p/P_s < 25, \tag{8}$$

$$\omega^* = 0.755 - 0.271(P_b^*/P_s) + 0.029(P_b^*/P_s)^2 - 0.001(P_b^*/P_s)^3 \tag{9}$$

The standard deviations of Eqs. (4)–(9) are 8.5%, 7.1%, 6.3%, 7.3%, 7.4%, and 6.8%, respectively. For the given primary-flow pressure and secondary-flow pressure, the critical (maximum) back pressure of the ejector required for stable operation can be calculated by Eq. (4), (6), or (8), and then the corresponding critical entrainment ratio can be calculated by Eq. (5), (7), or (9).

Figure 8 also gives comparisons of performance curves for different refrigerants—namely, steam, R113, and R114. The experimental conditions are P_p = 2.4–4.1 bar (T_p = 77–97°C) and Ma = 2.3, for R113, and P_p = 9.3–13.6 bar (T_p = 80–98°C) and Ma = 2.2, for R114 [7, 17]. The performance for R113 and R114 are better than that of steam in this condition. However, with the help of increasing Ma to 4.35 or 5.0 (corresponding to higher primary-flow pressures), the performance for the steam ejector is better than that of R114 and is comparable to that of R113. When the critical compression ratio P_b^*/P_s exceeds about 3.3, the performance for the steam ejector with Ma = 5.0 is even better than that of R113. For a Freon ejector, increasing ω^* with Ma is limited by practical design considerations for the endurable pressure of pressure vessels. It should also be noted that the required condenser temperature for a given P_b^*/P_s is lower for the steam ejector than for the Freon ejector, which means that a more efficient and larger condenser should be considered in the steam-ejector refrigeration system.

Two-Stage Ejector

The primary-flow pressures required to drive the ejector of Ma = 2.70 are relatively low at 80–200 torr, with the corresponding saturation temperatures at about 47–67°C. This indicates the potential use of low-grade heat, such as solar energy or waste heat from industrial plants. However, its available critical back pressures are still too low for the efficient operation of the condenser, particularly in summer. For example, for P_p = 200 torr and P_s = 10 torr, the available P_b^* is only 27.4 torr, corresponding to the

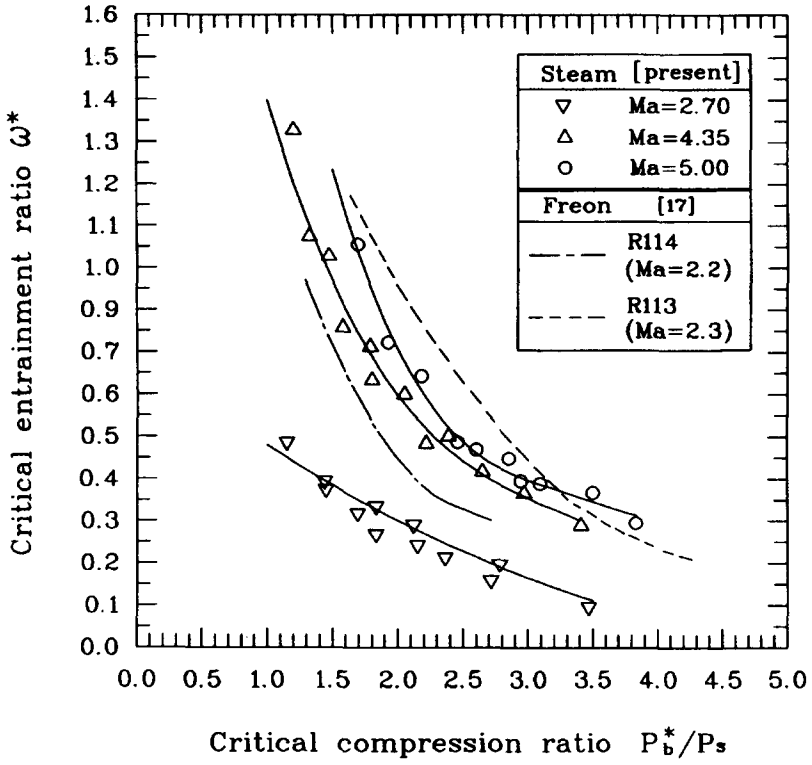

Figure 8. Comparison of operation performance for different exit Mach numbers and refrigerants.

saturation temperature of 27.5°C. To overcome this problem, a two-stage ejector was considered, and its configuration is presented in Fig. 9*a*. For a two-stage ejector, after a suitable intermediate pressure, P_i, is chosen, each stage can be treated independently [14]. Therefore, the performance of a two-stage ejector can be evaluated from the experimental results of single-stage ejectors obtained previously. The total critical entrainment ratio of a two-stage ejector, ω_t^*, is defined as

$$\omega_t^* = m_s/(m_{pA} + m_{pB}) = \omega_A^* \cdot \omega_B^*/(1 + \omega_A^* + \omega_B^*), \tag{10}$$

where ω_A^* and ω_B^* are the critical entrainment ratios for ejector A (first stage) and ejector B (second stage), defined as

$$\omega_A^* = m_s/m_{pB}, \tag{11}$$

$$\omega_B^* = (m_s + m_{pA})/m_{pB}. \tag{12}$$

Entrainment ratio ω_A^* can be calculated from Eq. (5), (7), or (9) by substituting P_i for P_b^*, P_s being the given secondary-flow pressure. On the other hand, ω_B^* is calculated by substituting P_i for P_s, and P_b^* being the given critical back pressure.

The evaluation results for two combinations are shown in Fig. 9*b*. For one combination (case 1), *Ma* is 2.70 for the first-stage ejector and 4.35 for the second-stage ejector. In the other (case 2), *Ma* for both stages is 2.70. The secondary-flow pressure, P_s, and critical back pressure, P_b^*, are held constant at 9.8 and 37.8 torr, respectively. Generally, the intermediate pressure is chosen to be between P_s and P_b^*. Therefore, compared with those of a single-stage ejector, the back pressure for the stable operation for the first-stage ejector is consequently decreased from P_b^* to P_i, and the entrainment ratio of the second-stage ejector is increased because its secondary-flow pressure has been increased from P_s to P_i. As shown in Fig. 9*b*, the total critical entrainment ratio of case 1 is much larger than that of case 2. The performance of case 1 is more sensitive to P_i than that of case 2, and an optimum P_i of about 20 torr exists for both cases.

With the use of the two-stage ejector, the required critical back pressure is increased and the low-grade heat can be practically used to drive ejectors (for case 2), although the total critical entrainment ratio is relatively low. At least, it can be used to enhance the entrainment ratio of the second-stage ejector (for case 1). This would be of considerable economic benefit, provided that the low-grade heat could be obtained inexpensively or even at no cost.

Description of Flow Structure

Further improvement of the ejector efficiency requires a greater understanding of its flow structure. Optical observation and measurement are thought to be the best methods for this purpose. Figure 10*a* shows a typical holographic interferogram of the ejector [18]. This picture would be a good indication of the flow field of a steam ejector, although it was obtained for an air ejector. As shown in Fig. 10, a diamond-like wave pattern is generated at the exit of the supersonic primary nozzle, because the exit pressure, P_x, is smaller than the secondary-flow pressure, P_s. An oblique shock appears again in the diffuser section owing to a choking condition at the constant area section. This behavior is consistent with the present measurements of the wall pressures in a steam ejector, as shown in Fig. 4*a*. Figure 10*b* is a schematic description of the flow structure together with that observed in a steam

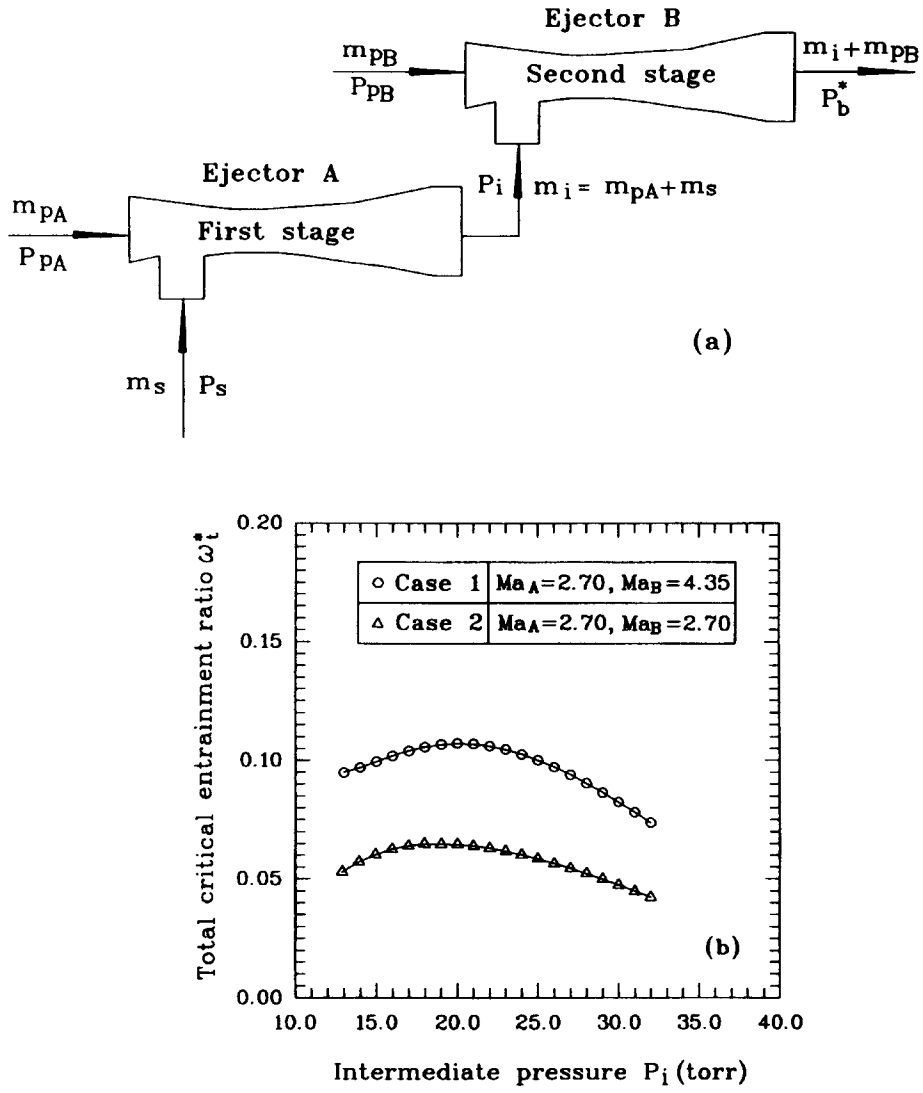

Figure 9. Configuration (*a*) and total critical entrainment ratio (b) of two-stage ejector.

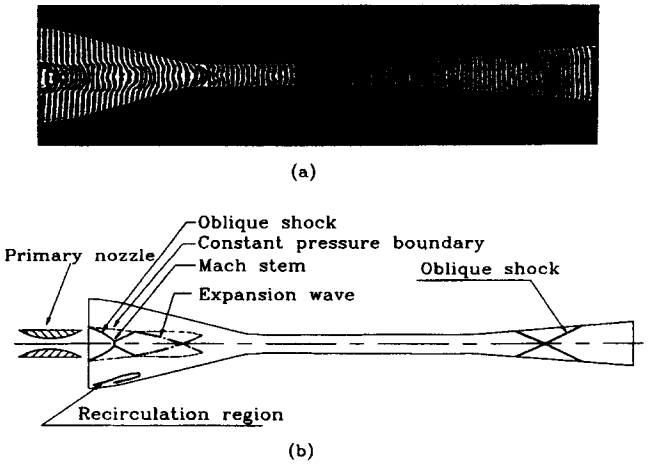

Figure 10. (*a*) Holographic interferogram of supersonic air-ejector [18]. (*b*) Schematic description of flow structure of ejector.

ejector in the present work. Water droplets repeatedly appear in the mixing section. The motion of these droplets implies that a circulating flow exists in the edge region, which seems to arise from the large velocity difference between the primary flow and the secondary flow. In addition, some smaller mists are retained at both the mixing section and the constant area section, but most of them are reevaporated and almost do not appear in the diffuser section. These condensed droplets and mists cannot be eliminated by increasing the superheat of primary-flow vapor even by as much as 10°C. The phenomenon of phase change (condensation) is more apparent with Ma = 4.35 than with Ma = 2.70, which can be attributed, at least partly, to the fact that a higher exit Mach number yields a smaller exit temperature at the primary nozzle.

Considering this observation, it may be necessary to reconsider the validity of the usual assumptions made in the theoretical analysis, including that the flow is one-dimensional or even axisymmeric, that the behavior of the fluid is like that of an ideal gas, and that the phase change due to heat interaction is not considered. However, such reconsideration would greatly increase the difficulties of

theoretical or numerical methods. Accordingly, in future work, we would like to further investigate the complicated flow structure of a supersonic steam ejector by holographic interferometry.

PRACTICAL SIGNIFICANCE

Not only can the experimental results help to understand the performance characteristics of a steam ejector, but the corresponding operation maps (Figs. 7–8) and empirical equations [Eqs. (4)–(9)] are useful for the practical design of steam-ejector refrigeration systems. For example, if $P_s = 12$ torr, $P_b^* = 36$ torr, and $Ma = 4.35$ are used, then the required motive pressure, calculated from Eq. (6), is 2.52 bar. Accordingly, the choking mass flow rate is calculated to be $m_p = 1.2 \times 10^{-3}$ kg/s by assuming an isentropic and one-dimensional flow. From Eq. (7), the entrained mass flow rate from the evaporator is determined to be $m_s = 4.5 \times 10^{-4}$ kg/s, and the generated refrigeration capacity is about $Q_e = 1$ kW. On the other hand, if one desires the refrigeration capacity to be larger or smaller for the foregoing conditions, the geometric dimensions of the ejector should be proportionally changed. For example, if $Q_e = 4$ kW is desired, then the required m_p must be increased by a multiple of four to $m_p = 4.8 \times 10^{-3}$ kg/s. Accordingly, the geometric dimensions including d_{t1}, d_{t2}, d_x, and the axial lengths of the three sections of ejector are all doubled ($= \sqrt{4}$) to 4.0, 35.6, 18.6, 214.0, 144.0, and 214.0 mm, respectively.

CONCLUSIONS

To experimentally investigate the performance characteristics of the steam-ejector refrigeration cycle, a relatively small scale system was built and tested at various operating conditions—namely, primary-flow pressure, P_p; secondary-flow pressure, P_s; and back pressure of the ejector, P_b. The effects including the exit Mach number, Ma, of the primary nozzle and the two-stage ejector also were evaluated. The following important conclusions can be drawn:

1. Both the critical entrainment ratio, ω^*, and the critical back pressure, P_b^*, are greatly affected by the operating conditions. For a given Ma and P_s, a larger P_p/P_s would yield a higher P_b^*/P_s but a lower ω^*. The effect of increasing Ma from 2.7 to 4.35 on P_b^* and ω^* is pronounced, and a further increase of Ma to 5.0 has only a slight effect. However, the required P_p is consequently increased by about three times. Accordingly, it seems to be unnecessary to excessively increase Ma, and 4.35 should be a moderate value for practical operation of a steam-ejector refrigeration system.
2. A comparison with other refrigerants reveals that the performance characteristics of the steam ejector itself are better than those of the R114 ejector and are comparable to those of the R113 ejector.
3. Primitive observation of the flow field reveals that there exist condensed droplets and mist, and a circulating flow is formed in the edge region of the mixing section. This indicates the necessity to further examine the flow structure of a steam ejector by experimental methods, among which holographic interferometry is suggested.

The authors acknowledge the financial support of the National Science Council, ROC, under Contract No. NSC 83-0413-E-002-004.

NOMENCLATURE

d	diameter, mm
Ma	exit Mach number of primary nozzle
m	mass flow rate, kg/s
P	pressure, bar or torr
Q	heat transfer rate, kW
T	temperature, °C
W_{mec}	mechanical power, kW

Greek Symbols

Δh	enthalpy difference, kJ/kg
ω	entrainment ratio

Subscripts

A	first-stage ejector
B	second-stage ejector
b	back condition of ejector
e	evaporator
g	generator
i	intermediate
p	primary flow
s	secondary flow
t	total condition
t1	primary nozzle throat
t2	ejector throat
x	exit of primary nozzle

Superscript

*	critical condition

REFERENCES

1. Zeren, F., Holmes, R. E., and Jenkins, P. E., Design of Freon Jet Pump for Use in Solar Cooling System, *ASME Paper No. 78 WA/SOL-15*, August, 1979.
2. Chen, F. C., and Hsu, C.-T., Performance of Ejector Heat Pumps. *Energy Res.* **11**, 289–300, 1987.
3. Sokolov, M., and Hershgal, D., Enhanced Ejector Refrigeration Cycles Powered by Low Grade Heat 1: Systems Characterization. *Int. J. Refrig.* **13**, 351–356, 1990.
4. Sokolov, M., and Hershgal, D., Enhanced Ejector Refrigeration Cycles Powered by Low Grade Heat 2: Design Procedures. *Int. J. Refrig.* **13**, 357–363, 1990.
5. Sokolov, M., and Hershgal, D., Enhanced Ejector Refrigeration Cycles Powered by Low Grade Heat 3: Experimental results. *Int. J. Refrig.* **14**, 24–31, 1991.
6. Sokolov, M., and Hershgal, D., Optimal Coupling and Feasibility of a Solar-Powered Year-Round Ejector Air Conditioner. *Solar Energy* **50**(6), 507–516, 1993.
7. Chen, S. L., Study on the Availability of Solar-Driven Ejector Refrigeration System. *EC, MOEA Report No. 812J4*, June, 1993 (in Chinese).
8. Steam-Jet Refrigeration Equipment. In *ASHRAE Equipment Handbook, ASHRAE*, Chap. 13, Atlanta, GA, 1979.
9. Keenan, J. H., Neumann, E. P., and Lustwerk, F., An Investigation of Ejector Design of Analysis and Experiment. *ASME J. Appl. Mech.* **17**, 299–309, 1950.
10. Chen, L. T., On the Design Theory of Constant-Area-Mixing Type Jet Compressors. *J. Chinese Inst. Eng.* **1**, 53–69, 1978.

11. Dutton, J. C., and Carroll, B. F., Optimal Supersonic Ejector Designs. *ASME J. Fluids Eng.* **108**, 414–420, 1986.
12. Vil'der, S. I., A Simplified Method of Calculating Stream-Jet Ejector Vacuum Pumps. *Int. Chem. Eng.* **4**(1), 88–92, 1964.
13. Rice, P., and Dandachi, J., An Equation for the Prediction of Steam Flowrate Required in the Design of Ejectors. *Chem. Eng. Res. Design* **69**(4), 332–334, 1991.
14. Sorensen, P. F., A. Thermodynamic Analysis of the Steam Ejector, Uranium Leach, Slurry-to Slurry Heat Exchanger. *Can. J. Chem. Eng.* **63**, 760–764, 1985.
15. Fort, J. F., and Heldmann, M. J., Development of a Recirculation Ejector for a Cryogenic Heat Sink for ECLSS. *SAE Trans.* **100**(1), 1154–1161, 1991.
16. Huang, M. C., The Analysis, Design, and Manufacturing of a Jet Refrigeration System, *Ph.D. Thesis*, Nat. Taiwan Univ., Taiwan, 1996.
17. Huang, M. C., and Chen, S. L., The Experimental Study of Ejector Performance Characteristic in Jet Refrigeration Systems. *Heat Recovery Syst. CHP* (submitted).
18. Chen, Y. M., and Sun, C. Y., Study on the Flow Field of a Supersonic Air-Ejector. *Proc. Symp. Transport Phenomena and Applications*, Taipei, pp. 17–20, September 1993 (in Chinese).

Received November 20, 1995; revised December 30, 1996